

1 **Microbially-accelerated weathering achieves carbon dioxide**
2 **removal by coupling silicate dissolution with carbonate precipitation**

3

4 **AUTHOR NAMES**

5 Corey R. Lawrence¹, Harun Niron², Tania Timmermann¹, Philip D. Weyman¹, Yun-Ya Yang¹,

6 Daniel Dores¹, Gonzalo A. Fuenzalida-Meriz^{1, *}

7

8 **AUTHOR ADDRESS**

9 ¹ Andes Ag, Inc., Alameda, California, USA

10 ² Biobased Sustainability Engineering (SUSTAIN), Department of Bioscience Engineering,

11 University of Antwerp, Antwerp, Belgium

12 * Corresponding Author: Gonzalo A. Fuenzalida-Meriz, gonzalofuenzalida@gmail.com

13 **ABSTRACT**

14 Microbial carbon dioxide mineralization (MCM) is a promising soil-based carbon dioxide removal
15 (CDR) strategy that leverages beneficial soil microbes to accelerate weathering of native silicate
16 minerals. This approach does not require addition of a mineral feedstock, greatly reducing the
17 carbon footprint from mining, grinding, transporting, and applying the mineral to land compared
18 with enhanced weathering. A key obstacle to measurement, reporting, and verification for MCM
19 is ensuring that weathering products are sourced from silicate dissolution rather than redistribution
20 of pre-existing cations from the exchangeable, oxidizable, or reducible soil pools. To address this,
21 we conducted a 63-day mesocosm study with soybean, utilizing soil sequential extractions to track
22 the buildup and distribution of weathering products in soil columns inoculated with *Bacillus*
23 *subtilis* strain MP1. Our results indicated that MP1-treated soils yield a net increase in available
24 base cations, corresponding to a 4.5% increase in base cation charge relative to control soils.
25 Increases in base cations were primarily partitioned between the carbonate and exchangeable soil
26 pools, with significant increases of carbonate in the MP1-treated soils. We also observed a small
27 but significant accumulation of silicon and magnesium in the reducible fraction, suggesting
28 secondary clay mineral formation. We estimate that 37% to 67% of the weathering-derived cations
29 formed carbonates, resulting in a CDR of 0.20 to 0.36 g CO₂ kg⁻¹ soil. These findings demonstrate
30 that *Bacillus subtilis* MP1 couples silicate mineral dissolution with carbonate precipitation,
31 confirming MCM as a viable CDR strategy.

32

33

34

35 **KEYWORDS**

36 carbon dioxide removal; microbial carbon dioxide mineralization; enhanced weathering; silicate
37 weathering; *Bacillus subtilis* strain MP1; soil inorganic carbon; carbonates

38

39 **HIGHLIGHTS**

- 40 ● Sequential selective extraction used to trace microbial acceleration of silicate weathering
41 in a soil mesocosm experiment with *Bacillus subtilis* strain MP1
- 42 ● Base cations in carbonate fraction were significantly greater in the microbially amended
43 soils compared to the controls.
- 44 ● Silicon and magnesium were also greater in the microbially amended soils columns.
- 45 ● Cation mass-balance indicates cation increases derive from silicate weathering, not
46 redistribution.
- 47 ● Microbial coupling of silicate weathering with carbonate precipitation support realized
48 CDR as soil inorganic carbon.

1 **1. INTRODUCTION**

2 In addition to reducing carbon emissions, technologies enabling carbon dioxide removal (CDR)
3 are needed to reduce the impact of anthropogenic greenhouse gas (GHG) emissions and meet the
4 demands of carbon markets (IPCC, 2022; Smith et al., 2024; Johnstone et al., 2025). Soil-based
5 CDR methods, such as enhanced weathering (EW) and microbial carbon dioxide mineralization
6 (MCM), are appealing because they can be applied in agricultural systems, resulting in co-benefits
7 for soil health and productivity, and where they can be efficiently scaled. The goal of EW is to
8 increase the dissolution of silicate minerals, which is a natural but slow process that acts as a
9 regulator of GHGs over millennial timescales (Walker, Hays & Kasting, 1981; Berner, 1997).
10 There are, however, economic and biogeochemical constraints on this approach that limit its
11 effectiveness in some soil environments. For example, most EW approaches work best in acidic
12 soils, and CDR must be high enough to offset emissions associated with the mining, grinding,
13 transport, and spreading of the feedstock material. Furthermore, the measurement, reporting, and
14 verification (MRV) required for issuance of high-quality carbon credits from soils can be difficult
15 to efficiently apply at scale. In the case of EW, this has led to a variety of different MRV
16 approaches, each with unique costs and benefits (e.g., Clarkson et al., 2024). It is becoming
17 increasingly apparent that there is no ‘one size fits all’ approach. Technological innovation coupled
18 with applied research will continue to be essential for achieving CDR at the scale required to
19 combat climate change.

20

21 Weathering of silicate minerals contained in rocks and soil is a natural negative-feedback to
22 increasing atmospheric CO₂, whereby carbonic acid formed from CO₂ and water supplies the
23 acidity needed to drive mineral dissolution. As silicates dissolve, base-cations contained within

24 the minerals are released to solution, and carbon from carbonic acid is converted to carbonate
25 alkalinity (i.e., $\text{HCO}_3^- + \text{CO}_3^{2-}$). In natural settings, these reactions are assumed to be too slow to
26 effectively offset anthropogenic GHG emissions over human timescales. EW approaches increase
27 weathering rates by adding finely crushed mineral feedstocks to soils, accelerating effective
28 weathering rates by increasing the mineral surface area. However, it is becoming increasingly clear
29 that mineral weathering is not strictly an abiotic process; microbes, including bacteria and fungi,
30 have been shown to facilitate and enhance rates of mineral weathering (Finlay et al., 2020; Vicca
31 et al., 2022; Wild et al., 2022; Banfield et al., 1999; Verbruggen et al., 2021; Timmermann et al.,
32 2025; Corbett et al., 2025). There are several hypothesized mechanisms through which microbes
33 may increase mineral weathering, including exudation of carbonic anhydrase enzymes that
34 enhance the solubility of CO_2 and formation of carbonic acid (Xiao et al., 2015; Vicca et al., 2022;
35 Timmermann et al., 2025) or through exudation of organic acids that supply acidity for weathering
36 and act as ligands that remove weathering products (Ribeiro et al., 2020; Vicca et al., 2022; Niron
37 et al., 2025). Harnessing this biological potential may provide another valuable tool to accelerate
38 and scale CDR.

39
40 Microbe-based approaches for accelerating silicate weathering, such as MCM, can be applied to
41 soil systems without the addition of exogenous mineral feedstocks (Timmermann et al., 2025). By
42 increasing weathering of preexisting silicate minerals, upfront costs and carbon emissions can be
43 reduced, allowing for more efficient and cost-effective CDR. However, this approach requires
44 soils meeting specific geochemical conditions, and soils must be (1) rich in cation-bearing silicate
45 minerals to be weathered, (2) neutral to alkaline pH (discussed in Yang et al., 2026), and (3) able
46 to precipitate products of mineral dissolution as secondary carbonates. Timmermann et al. (2025)

47 proposed that accumulation of secondary carbonate minerals, facilitated by microbial
48 amendments, serves as an effective proxy for weathering, allowing for MRV approaches based on
49 carbon rather than base cations. When carbonate formation is coupled with the dissolution of
50 silicates containing divalent cations (Mg^{2+} and Ca^{2+}), which consume two moles of CO_2 for every
51 mole of mineral weathered, half of the CO_2 removed is returned to solution. Carbonate formation
52 therefore reduces the efficiency of CDR from silicate weathering, which is why it is undesirable
53 in traditional EW systems. Yet, without the need for mining, crushing, and transporting feedstock
54 and the associated CO_2 emissions, this process can still allow for cost-effective CDR in a system
55 where only microbial amendments are added to a soil. However, one potential concern with such
56 an approach is that increases in secondary carbonate accumulation could conceivably occur
57 without corresponding increases in silicate weathering, for example, if the divalent cations
58 precipitated in carbonates are sourced from somewhere else in the soil system (e.g., the
59 exchangeable complex). To address this concern and definitively link microbial amendments with
60 increases in silicate dissolution, we conducted an experiment leveraging sequential selective soil
61 extraction, a technique allowing for a comprehensive characterization of the soil weathering
62 system, including tracking of all potential sinks for weathering products (e.g., Steinwidder et al.,
63 2026).

64
65 In this study, we describe the results of a laboratory mesocosm experiment, where soybeans were
66 grown with and without the addition of a microbial amendment, *Bacillus subtilis* MP1. We have
67 previously demonstrated that, in both laboratory and field experiments, when soils are amended
68 with strain MP1 or similar microbes, the microbial-acceleration of silicate mineral dissolution can
69 facilitate CDR (Timmermann et al., 2025; Niron et al., 2024). Additionally, we have shown the

70 potential for these microbial amendments to improve the effectiveness of EW when microbes are
71 added in combination with silicate feedstocks (Yang et al., 2026). However, in both microbial
72 amended and traditional EW systems, questions remain regarding the fate of weathering products,
73 including base-cations and carbonate alkalinity. We used a sequential selective soil extraction
74 procedure (e.g., Niron et al., 2024; Vienne et al., 2025; Steinwider et al., 2025) to trace how the
75 microbial amendment MP1 altered silicate weathering and changed various soil base-cation pools.
76 Data from selective sequential extractions provide a powerful way to track products of silicate
77 dissolution and the potential sinks of weathering products. By tracking all inputs and reservoirs of
78 base cations in the experimental system, along with inorganic carbon and other diagnostic soil
79 properties, this work clearly demonstrates that the microbial amendment MP1 facilitates carbonate
80 accumulation by increasing the dissolution of silicate minerals.

81

82 **2. MATERIALS AND METHODS**

83 **2.1. Soil mesocosm experiment.** A 63-day soil mesocosm experiment was conducted using 12
84 soil columns to assess the impact of the microbial amendment *Bacillus subtilis* strain MP1, on soil
85 silicate weathering under soybean (*Glycine max*) cultivation. The soil used for the mesocosm
86 experiment, hereafter referred to as SBX70, was a silty clay soil collected from an agricultural
87 field in Stutsman County, North Dakota, USA. Prior to the mesocosm preparation, the SBX70 soil
88 was sieved through a 10 mm mesh to remove large stones and plant debris, and then manually
89 homogenized. Each mesocosm (35 cm height and 10 cm diameter) was filled with 3 kg of field-
90 moist SBX70 soil to a total height of 30 cm, leaving 5 cm of headspace. After correcting for the
91 moisture content of the soil, this equated to a dry mass of 2.18 kg within each mesocosm.

92 The experimental design consisted of two treatment groups, each with six biological replicates: (i)
93 untreated control (“UTC”) and (ii) MP1 inoculated (“MP1”) (Figure S1). MP1 is a naturally
94 occurring *B. subtilis* strain isolated from corn roots and rhizosphere soils. Detailed characterization
95 of MP1 can be found in Timmermann et al. (2025). Each mesocosm was planted with a single
96 soybean seed (Asgrow AG19XF3). To prepare the MP1 treatment, each seed was inoculated with
97 3.9×10^6 spores of MP1 suspended in 1 mL of distilled water. The concentration of MP1 spores
98 added per mesocosm equates to 3.9×10^3 spores per gram of soil. In the UTC treatment, 1 mL of
99 distilled water per seed was applied instead. The experiment was conducted in a growth chamber
100 under the following conditions: temperature of 22 °C (± 5 °C), relative humidity of 65% ($\pm 5\%$),
101 and a 16-hour photoperiod. Plants were watered with deionized (DI) water three times a week for
102 the first six weeks.

103

104 **2.2. Simulated rainfall events and sample collection.** Six weeks (42 days) after sowing and MP1
105 inoculation, six simulated rainfall events were applied to the mesocosms over a two-week period.
106 The total rainfall amount was 1.75 L of DI water per mesocosm, distributed across the six events,
107 with each mesocosm receiving 292 mL DI water per event. The total volume of water was
108 determined as described in Timmermann et al. (2025). The simulated rainfall schedule followed a
109 pattern of two consecutive days of water additions, followed by two days without, repeating three
110 times, for a total of six simulated rainfall events. Leachate was collected from each mesocosm
111 during each of the six discrete rainfall events, thereby accounting for the total leachate flux
112 throughout the experiment. Following the simulated rainfall period, plants continued to grow under
113 controlled conditions until day 63, at which point they were harvested.

114

115 After the 63-day experiment, all 12 mesocosms were harvested and soils were divided into three
116 depth intervals for analyses: 0–10 cm, 10–20 cm, and 20–30 cm (Figure S1). A total of 36 soil
117 samples (two treatments with six replicates and three depths per replicate) were collected and
118 homogenized. Then, the samples were air dried, sieved to 2-mm, and ground for soil
119 physicochemical analyses. Soybean plants were harvested separately for aboveground and
120 belowground biomass.

121

122 **2.3. Soil chemistry.** The total elemental composition of the SBX70 soil prior to the onset of the
123 experiment was measured via x-ray fluorescence (XRF) at the GeoAnalytical Laboratory at
124 Washington State University (Pullman, WA, USA), and soil organic matter content was
125 determined by the loss-on-ignition method at 360 °C (Combs & Nathan, 1998) to allow for
126 normalization of the elemental composition on a volatile-free basis. Technical details and
127 principles underlying these methods are described in Johnson et al. (1999) and Kelly (2018).

128 Soil inorganic carbon (SIC) was quantified using a gas chromatography (GC) method described in
129 Yip et al. (2025). Soil bicarbonate (HCO_3^-) and carbonate (CO_3^{2-}) ions were quantified using a
130 saturated paste extract followed by titration (Richards L.A., 1954; Yang et al., 2026). Due to the
131 complexity of this measurement, the saturated paste extract was made on a single depth-
132 composited sample from each column. In this study, “carbonate alkalinity” is defined as the
133 combined concentration of HCO_3^- and CO_3^{2-} ions in the soil.

134

135 Additional soil physicochemical parameters were analyzed by an external commercial laboratory
136 (Agvise Laboratories, ND, USA). Soil pH was measured using the standard 1:1 soil-to-water ratio
137 method with a calibrated pH meter (Peters et al., 2012). Soil total carbon (TC) was quantified via

138 dry combustion using a Vario MACRO cube elemental analyzer (Elementar Americas Inc., NY),
139 while total soil organic carbon (SOC) was calculated as the difference between TC and SIC
140 (Nelson & Sommers, 1996). Total soil cation exchange capacity was measured using the
141 ammonium acetate displacement method (Sumner & Miller, 1996) and was compared against the
142 sum of exchangeable base cations (described below) to estimate base saturation of the exchange
143 complex, where base saturation (%) is equal to the sum of exchangeable base cations divided by
144 the total cation exchange capacity (both in units of mEq/100g soil).

145

146 **2.4. Sequential cation extractions.** Four soil cation pools were sequentially extracted from soil
147 samples to assess changes in cation mobility and distribution: (1) exchangeable cations, (2)
148 carbonate-bound cations, (3) reducible cations, and (4) the oxidizable fraction. Methodology for
149 sequential extractions was adapted from Tessier et al. (1979) and Uhlig & von Blanckenburg
150 (2019), and is detailed in Steinwidder et al. (2025). In the first step (exchangeable cations), 10 mL
151 of 1 M NH₄OAc was added to 1 g of air-dried soil, shaken for 1 h, centrifuged, and the supernatant
152 collected. For the second step (carbonates), 5 mL of 1 M CH₃COOH was added and shaken for
153 2 h; then 1 mL of 3 M NH₄OAc was added. Samples were brought to 10 mL with DI water,
154 centrifuged, and supernatants collected. In the third step (reducible — oxide/hydroxide bound
155 cations), 5 mL of 0.05 M NH₂OH in 1 M HCl was added. Samples were heated at 80 °C for 5 h
156 with manual shaking every 30 min, then treated with 3 M NH₄OAc, diluted to 10 mL, centrifuged,
157 and collected. In the final step (oxidizable — organic-bound cations), 4 mL of 30% H₂O₂ in 0.01M
158 HNO₃ was added, and samples were heated at 70 °C with periodic shaking. After 2 h, 3 mL more
159 H₂O₂ was added, and heating continued for 3 h. Then 1 mL of 3 M NH₄OAc was added, samples

160 were diluted to 10 mL, centrifuged, and collected. Between each step, the soils were rinsed with
161 10 mL of DI water. All centrifugations were done at 4000 rpm for 10 min, and all extracts were
162 filtered through 0.45 μm filters.

163
164 Elemental concentrations were measured using ICP-OES (iCAP 6300 Duo, Thermo Scientific) for
165 Ca, Mg, K, and Na in all cation pools, and for Al, Fe, and Si in the last two pools. Samples were
166 acidified (19:1, 2% HNO_3 :sample; TraceMetal Grade, Fisher Chemical) prior to analysis.
167 Calibration used a multi-element standard (CPAChem), with yttrium (Merck) as the internal
168 standard. All standards were diluted in the respective extraction media to ensure matrix-matched
169 calibration and sample conditions.

170
171 **2.5. Plant biomass & chemistry.** At the end of the experiment, above and belowground plant
172 biomass was harvested from each column. Samples were oven dried at 60 $^{\circ}\text{C}$, then weighed prior
173 to grinding for chemical analyses. Aboveground dry biomass samples were analyzed for elemental
174 composition by ICP-OES following acid digestion at Agvise Laboratories (Northwood ND, USA).
175 Due to lower sample mass from individual columns, an equal mass of belowground biomass from
176 replicate columns were combined, yielding two pooled samples per treatment. The belowground
177 biomass samples were analyzed by ICP-OES following acid digestion at The Pennsylvania State
178 University Agricultural Analytical Service Laboratory (State College PA, USA). To calculate the
179 total cation content attributable to plant above and belowground biomass, measured cation
180 concentrations in plant tissue (mg/kg) were multiplied by plant tissue dry weight.

181

182 **2.6. Leachate chemistry.** Leachate samples, collected from mesocosms following each simulated
183 rainfall event, were analyzed for several biogeochemical parameters. Leachate pH was measured
184 with a benchtop probe following a multipoint calibration. Bicarbonate and CO_3^{2-} ions were
185 quantified via titration with 0.0125 M H_2SO_4 with phenolphthalein and methyl orange indicators
186 (Richards L.A., 1954). Dissolved inorganic carbon (DIC) in leachate was measured on 4 mL of
187 sample following the GC method described in the previous section. Remaining leachate samples
188 were stored frozen and submitted to Agvise Laboratories (Northwood, ND, USA) for analysis of
189 concentrations of soluble cations Ca^{2+} , Mg^{2+} , K^+ , and Na^+ (APHA, 1998) as well as major anions
190 including NO_3^- , SO_4^{2-} , and Cl^- . Soil leachate data was assessed for charge balance. Positive charge
191 offsets were assumed to result from sample re-equilibration during the collection phase and were
192 corrected by adjusting total carbonate alkalinity ($\text{HCO}_3^- + \text{CO}_3^{2-}$) by the corresponding magnitude
193 of the offset (Tosca & Tutolo, 2023).

194

195 **2.7. Statistical analyses.** Based on the distribution and homoscedasticity of the data, either a
196 parametric Student's t-test (normal distribution and equal variance) or a nonparametric Mann–
197 Whitney U test (Wilcoxon rank-sum) was applied to evaluate significant differences ($p < 0.05$) in
198 soil properties among treatments. Statistical analyses of soil and water physicochemical properties
199 were performed using the GraphPad Prism version 10 (GraphPad Software, Boston,
200 Massachusetts, USA) or using tools from the tidyverse packages (Wickham et al., 2019) in R
201 (v4.5.0, R Core Team, 2021).

202

203 **3. RESULTS**

204 **3.1 Bulk soil and leachate chemistry**

205 3.1.1. Soil and leachate pH

206 The initial pH of the SBX70 soil was 7.1 ± 0.03 ($N = 3$). The volume weighted pH of column
207 leachate was significantly higher ($p < 0.05$, $N = 6$) from the MP1 treatment (8.44 ± 0.04), showing
208 an increase of 0.14 in comparison to the untreated control (8.30 ± 0.06) (Figure 1A). At the end of
209 the experiment, the mean value of soil pH was higher for MP1-treated columns compared with
210 UTC, but the difference was not statistically significant (Figure 1B).

211

212 3.1.2. Alkalinity and inorganic carbon in soil and leachate

213 At the end of the 63-day experiment, soil carbonate alkalinity ($\text{CO}_3^{2-} + \text{HCO}_3^-$), measured from
214 soil titrations, was significantly higher ($p < 0.05$, $N = 6$) in MP1 compared with UTC columns
215 (Figure 2A). Alkalinity in leachate is reported as the total cumulative flux normalized by the mass
216 of soil in each column (mEq/kg soil) so that it can be directly compared to soil measurements.
217 Leachate alkalinity was similar between treatments, thus, differences between treatments in the
218 total alkalinity of the system (soil + leachate), were mainly driven by the solid phase, resulting in
219 a higher total alkalinity for MP1-treated soils in comparison to UTC soils (Figure 2A).
220 Inorganic carbon in leachate and soil showed similar trends, with
221 higher mean values of SIC and TIC in the MP1 treated columns ($\approx 37\%$
222 increase over UTC) (Figure 2B).

223

224 3.1.3. Soil total, inorganic and organic carbon

225 Total soil organic carbon (SOC) from the MP1-treated soil was significantly greater than UTC in
226 the 20-30 cm soil increment ($p < 0.05$, $N = 6$) (Figure 3A). Total inorganic carbon (TIC)
227 concentrations were near the detection limit of our method for all soils in this study, and though

228 not significant, mean values of MP1-treated soils were consistently higher in TIC across all depth
229 increments (Figure 3B), and at the column level (Figure S2B). When considering the entire
230 column, total carbon was significantly higher ($p < 0.05$, $N = 6$) in the MP1 treatment versus UTC
231 (Figure 3C), and with depth resolution, significant increases in the MP1-treated soils were
232 observed in the 20-30 cm increment (Figure S2A).

233

234 **3.1.4. Soil cation exchange capacity and column base cation fluxes**

235 Values of total cation exchange capacity ranged from roughly 40 to 47 mEq/100g soil across all
236 treatments and depths, and no clear patterns or significant differences were observed (Figure S3).
237 The total flux of cations in column leachate (calculated as leachate volume collected x
238 concentration) was 5% higher in the MP1 treatment, and all individual base cations were higher in
239 MP1 compared to UTC samples, but differences were not statistically significant (Figure S4).

240

241 **3.1.5. Plant cation content**

242 Plant biomass was slightly elevated in UTC compared with MP1 columns, but the concentration
243 of base cations tended to be higher in plants from the MP1 column, though neither trend was
244 statistically significant (data not shown). As a result, the overall mass of individual base cations
245 attributable to plant matter was similar for both UTC and MP1 treatments. There were no
246 significant differences observed for the total mass of Mg and K between treatments. The total mass
247 of Ca was higher in MP1 treatment compared with UTC ($p < 0.1$); however, Na was significantly
248 lower in the MP1 treatment compared with UTC ($p < 0.05$, Figure S9).

249

250 **3.2. Sequential extractions results**

251 **3.2.1. Exchangeable fraction**

252 There were no significant differences in exchangeable base cations between treatments, though
253 mean values of exchangeable Ca were consistently higher in MP1-treated columns compared with
254 UTC across all soil depths (Figure S5). Differences in base saturation, calculated as the ratio of
255 the sum of exchangeable base cations to the total cation exchange capacity, were not statistically
256 significant but the mean values were consistently higher for MP1-treated versus UTC columns
257 (Figure S6).

258

259 **3.2.2. Carbonate fraction**

260 The carbonate extraction yielded some significant differences between MP1 and UTC treatments.
261 In the 10 to 20 cm depth increment, all base cations (Ca, Mg, K, and Na) were significantly higher
262 in the MP1 treatment (Figure 4). Concentrations of K were also significantly greater in the 0-10
263 and 20-30 cm depth increments.

264

265 **3.2.3. Reducible fraction**

266 Except for Na in the 10-20 cm depth increment, which was significantly higher in the MP1-treated
267 columns, masses of elements extracted from the reducible pool were comparable between the MP1
268 and UTC treatments of the top two depth increments (Figure S7). In contrast, masses of Mg and
269 Si extracted from the reducible pool of the 20-30 cm depth increment were significantly greater in
270 the MP1-treated columns compared with UTC (Figure 5). The mean values of all other elements
271 measured (Al, Fe, Ca, K, and Na) were also higher in the MP1-treated columns but differences
272 were not significant at the $p < 0.05$ threshold. The normalized molar ratio of Fe:Mg:Si found in

273 the reducible fraction of both treatments was on the order of 1:2.5:4 consistent with Si-Mg rich
274 Fe-(hydr)oxides.

275

276 **3.2.4. Oxidizable fraction**

277 With one exception, there were no significant differences in elemental masses extracted from the
278 oxidizable pool of the MP1 and UTC columns (Figure S8). The exception was Na in the 10 to 20
279 cm increment, which was near the detection limit for all MP1 columns.

280

281 **3.3. Cation mass-balance**

282 At the end of the 63-day experiment, the total mass of base cations recovered across all
283 biogeochemical pools measured in this study was higher in the MP1-treated soils compared with
284 UTC soils, for Ca, Mg, and K (Figure 6). In contrast, the total amount of Na recovered was higher
285 in the UTC soils. For Ca and Mg, the two dominant cations in the system, the exchangeable pool
286 represented the largest proportion of the total recovered mass, followed by the carbonate pool (for
287 Ca) and reducible pool (for Mg). Only a small fraction of these cations was associated with the
288 oxidizable, plant biomass, or leachate pools. The pattern for K was consistent with those observed
289 for Mg: most of the recovered K resided in the exchangeable and reducible pools. Whereas the
290 pattern for Na was consistent with those observed for Ca: the two dominant pools were the
291 exchangeable and the carbonate pools. Contrary to the other three cations, the amount of Na
292 recovered from the reducible pool was negligible (Table S3).

293

294 **4. DISCUSSION**

295 **4.1. A conceptual framework for microbe-mediated weathering**

296 Leveraging the soil microbiome to promote carbon dioxide removal represents a promising
297 approach to help offset anthropogenic carbon emissions (Fierer & Walsh, 2023). One such strategy
298 involves using microbes to increase silicate mineral weathering, which converts atmospheric CO₂
299 to HCO₃⁻ and carbonates. For example, previous experiments using the plant growth-promoting
300 rhizobacterium *B. subtilis* MP1 (Timmermann et al., 2025; Yang et al., 2026) or other *Bacillus*
301 *subtilis* strains (Corbett et al., 2025; Niron et al., 2024; Hopf et al., 2009; Song et al., 2007) have
302 suggested promising increases in mineral weathering rates in both laboratory and field
303 environments. This highlights the potential use of microbial amendments as a CDR strategy, and
304 it is hypothesized that increases in mineral weathering driven by these microbes support plant
305 growth through acquisition of rock-derived nutrients (e.g., P, Ca, Mg, K), which are essential for
306 plant growth (Samuels et al., 2020; Dong et al., 2022).

307
308 Timmermann et al. (2025) presented a conceptual framework for how these microbes may drive
309 silicate mineral weathering. In this model, microbes facilitate the production of acidity (H⁺) via
310 carbonic anhydrases driven catalysis of the conversion of CO₂(aq) to HCO₃⁻ (e.g., Supuran, 2016)
311 and precipitation of carbonate (which also generates H⁺). The protons generated are directed across
312 the microbial biofilm toward the mineral surface where weathering occurs, and the products of
313 weathering are mobilized away from the mineral to facilitate continued dissolution (Figure 4 in
314 Timmermann et al., 2025). This conceptual framework has support in the literature
315 (McConnaughey & Whelan, 1997) but has yet to be fully validated in the context of microbially-
316 mediated weathering. Experimental evidence provides support for the role of secondary carbonate
317 formation in the context of MP1 amendment (Timmermann et al., 2025). Nonetheless, one concern
318 is that the observed increases in soil carbonate associated with the microbial amendment may

319 source divalent cations from somewhere other than the silicate weathering. To address this
320 question, we conducted a soil mesocosm experiment following the approach described in
321 Timmermann et al. (2025) and Yang et al. (2026), this time incorporating a sequential selective
322 extraction procedure (e.g., Niron et al., 2024; Vienne et al., 2025; Steinwidder et al., 2025; 2026)
323 to trace base cations in available soil reservoirs.

324

325 **4.2. Bulk soil response to MP1 amendment**

326 Despite being well suited for the MCM approach, with roughly 28% (v/v) feldspars and an initial
327 soil pH of 7.13, the impact of the MP1 microbe amendment was not entirely apparent from bulk
328 soil and leachate data. The flux-weighted pH of the soil leachate was significantly higher from the
329 MP1 columns (Figure 1A), implying a greater consumption of protons, possibly through increased
330 weathering. Soil pH was also elevated in the MP1 treatment compared with control, though
331 differences were not significant (Figure 1B). Similarly, carbonate alkalinity and inorganic carbon
332 content were each higher in the MP1-treated columns (Figure 2), but only soil alkalinity was
333 significant. There were no significant differences in the leachate flux of alkalinity, inorganic
334 carbon, or base cations (Figures 2 and S4). Organic carbon content was significantly higher in the
335 20-30 cm depth increment (Figure 3A) and, when summed across the entire column, there was
336 significantly greater total carbon in the MP1-treated soils (Figure 3C). Overall, these data provide
337 evidence of increased weathering (higher pH and soil carbonate alkalinity) and total soil carbon
338 associated with MP1 additions. These findings are similar to those presented in Yang et al. (2026),
339 and despite patterns suggesting a consistent response to the MP1 amendment, the 63-day
340 experiment may not have been long enough relative to the effect size (Hasemer et al., 2024). By

341 further partitioning the soil into pools or fractions via sequential selective dissolution, we improve
342 our ability to understand these suggestive but inconclusive bulk soil data.

343

344 **4.3. Cation tracing suggests retention of weathering products in secondary minerals**

345 Selective dissolution is a well-established tool for understanding the distribution of elements
346 across a variety of mineralogic, biologic, or geochemical soil fractions in soils and sediments
347 (Heckman, Lawrence, & Harden, 2018; Wagai & Mayer, 2007; Tessier et al., 1979; and many
348 others). Although there are some potential pitfalls when using such an approach to compare across
349 different soils (e.g., Hass & Fine, 2010; Martin, Nirel, & Thomas, 1987), when applied to a
350 controlled laboratory experiment, partitioning elements between soil ‘fractions’ or ‘pools’
351 provides additional information about sources and sinks associated with changes in the overall
352 system chemistry in response to a treatment. In the context of silicate weathering, this information
353 can be further used to understand the potential implications for CDR (te Pas et al., 2025). The
354 sequential extraction data indicated significant increases in base cations within the carbonate
355 (Figure 4) and reducible (Figure 5) fractions of the MP1-treated columns, with no change in the
356 exchangeable (Figure S5) or oxidizable (Figure S8) fractions.

357

358 Given that cation enrichment in carbonate and (hydr)oxides was not accompanied by decreases
359 from any fractions in the MP1-treated columns, remobilization from other depths or fractions is
360 ruled out as a source for the observed increases. Rather, the excess cations, as well as Si and Fe in
361 the reducible fraction, are likely derived from a reservoir not directly quantified with the sequential
362 extraction, with the most likely source being cation-bearing silicate minerals. Increases in Fe and

363 Mg in the reducible fraction are frequently observed following basalt additions (e.g., Niron et al.,
364 2024; Vienne et al., 2025).

365

366 The depth dependence of the observed carbonate (10-20 cm) and reducible fraction base cation
367 enrichments (20-30 cm) within the MP1-treated columns suggest that microbially-enhanced
368 weathering could be spatially variable or that the secondary phases were influenced by the reactive
369 transport and accumulation of weathering products. We did not quantify root abundance with
370 depth, which could have provided insight to the depth distribution of rhizosphere activity.
371 However, because soil respiration generally results in $p\text{CO}_2$ values well above atmospheric levels
372 and the mesocosms are open on the top and bottom, it is reasonable to expect that soil $p\text{CO}_2$ was
373 highest in the intermediate depth. The observed patterns of carbonate and reducible enrichment
374 are consistent with the accumulation of weathering products as porewater infiltrates through the
375 columns. Given that there were no significant differences observed between the treatments in the
376 leachate flux of base cations, it appears that the products of microbially-enhanced weathering were
377 largely retained within the soils.

378

379 The accumulation of weathering-derived base cations in soil pools, sometimes referred to as
380 ‘cation-scavenging,’ influences whether or not the associated CDR is realized (Vienne et al., 2025;
381 Bijma et al., 2026; te Pas et al., 2025; Steinwidder et al., 2025; Hasemer et al., 2024). For the
382 purpose of durable CDR, the ideal scenario is that base cations generated from silicate mineral
383 dissolution are exported from the system in the soil porewater, along with the negatively charged
384 carbon alkalinity. Due to the constraint of charge balance in solution, when base cations generated
385 from weathering are retained within the soil, the corresponding alkalinity is also retained, and in

386 some cases (e.g., acidic soils) can be converted back to CO₂. However, not all soil sinks for base
387 cations are equivalent (Figure 7). The formation of carbonate minerals results in realized CDR,
388 but only half of what would occur if alkalinity was exported. On the other hand, sequestration of
389 base cations in the exchangeable or oxidizable pools are assumed to delay CDR because those
390 cations can eventually be released and exported (Figure 7). Finally, when base cations accumulate
391 in the reducible pool including secondary hydr(oxides) and clays, or are taken up by plants, CDR
392 is inhibited (te Pas et al., 2025; Vienne et al., 2025; Steinwidder et al., 2025).

393
394 The molar ratios of Fe, Mg, and Si in the reducible fraction were generally consistent with
395 formation of Si-Mg rich Fe-(hydr)oxides, which could be a precursor to smectite clays. The
396 eventual formation of smectite would be consistent with normal weathering in these North Dakota
397 soils (Franzen & Bu, 2023). Although both Fe-(hydr)oxides and smectite tend to have high cation
398 exchange capacity (compared with primary silicates), we did not see significant increases in CEC
399 at any depth in the MP1 treatment (Figure S2). However, we did observe a significant increase in
400 organic carbon in the 20-30 cm increment (Figure 3), which could be related to increased
401 (hydr)oxides as suggested by the reducible fraction data. While more work is needed to definitively
402 identify the minerals associated with the reducible fraction and the possible implications for SOC,
403 it is worth noting, compared with EW approaches where exogenous mineral feedstock are applied
404 to the soil, the MCM approach is less likely to generate new forms of secondary minerals that were
405 not already present in the soil.

406

407 **4.4. The importance of carbonate precipitation in microbially-accelerated weathering**

408 The higher base cation content in the carbonate pool of the MP1-treated columns is consistent with
409 increases in soil carbonate reported in Timmermann et al. (2025) and provides another line of
410 support for the conceptual model presented above, whereby carbonate precipitation is linked to
411 microbially-enhanced silicate weathering. In addition to generating acidity, carbonate formation
412 can serve as a sink for weathering products and could maintain higher rates of weathering by
413 limiting reductions in reaction affinity associated with the accumulation of weathering products
414 (i.e., Maher et al., 2009).

415

416 It is noteworthy that the sequential extraction results showed a significant increase in the carbonate
417 fraction from 10-20 cm in MP1 treatment, whereas bulk SIC increases in the MP1 treatment were
418 not significant (Figure S2B). This difference could derive from higher variability of SIC compared
419 with the sequential extraction base cation data, or from SIC values approaching analytical
420 detection limits. The SIC measurements are highly correlated with the total base cations in
421 carbonate extraction (Pearson's $r = 0.89$, $p < 0.0001$) but estimates of additional carbonate in the
422 MP1 columns from SIC measurements (0.018 mol CaCO_3 per column) were higher than the
423 sequential extraction base cation estimates (0.010 mol CaCO_3 per column). We attribute this
424 difference to the partial dissolution of newly formed carbonates during the exchangeable cation
425 extraction. Although 1.0 M NH_4OAc is widely used to estimate exchangeable cations, it is known
426 to partially dissolve carbonates under some conditions (Tessier et al., 1979; Nel, Bruneel, &
427 Smolders, 2022), potentially leading to an overestimation of exchangeable Ca and Mg and to a
428 corresponding underestimation in the carbonate pool. Furthermore, newly formed biogenic
429 carbonates (e.g., beta calcretes) tend to be fine grained and may be more prone to partial dissolution
430 (Domínguez-Villar et al., 2022; Wright et al., 1989). Because selective sequential extractions can

431 be susceptible to over- or under-extraction (Hass & Fine, 2010), we assume the SIC-based
432 estimates to be the more accurate measure of the magnitude of soil carbonate.

433

434 Based on the mass balance calculations, increases in Ca from the microbial acceleration of silicate
435 weathering was primarily partitioned between the carbonate and exchangeable soil fractions
436 (Figures 6 and 7). However, as discussed above, the sequential extraction method may
437 overestimate the amount of weathering-derived base cations in the exchangeable fraction at the
438 expense of the carbonate fraction. Together these two pools account for the majority of new cations
439 generated through silicate weathering in this soil. The mass of exchangeable Ca (Figure S5) as
440 well as base saturation of the exchange complex (Figure S6) trended higher in the MP1-treated
441 columns but these patterns were not statistically significant, suggesting they may be difficult to
442 detect due to natural soil heterogeneity. Furthermore, in soils with a higher initial base saturation
443 (e.g., Timmermann et al., 2025), we would expect a larger proportion of new Ca to end up in the
444 carbonate fraction. In other words, the base saturation of the soil will influence the efficiency of
445 the carbonate sink, with higher initial degrees of base saturation likely resulting in more carbonate.

446

447 There is a large body of evidence demonstrating microbially induced carbonate precipitation by
448 an array of different microbes including *Bacillus subtilis* (Zhu & Dittrich, 2016 and reference
449 therein). Moreover, we have previously demonstrated that *B. subtilis* MP1 increases the rate of
450 carbonate precipitation in an alkaline soil (Timmermann et al., 2025). It follows that carbonate
451 precipitation likely occurs in proximity to the MP1 biofilms, and that base cations incorporated
452 within the newly formed carbonates could be removed from solution before they can react with
453 the exchange complex or other cation sinks within the soil. If true, when compared to EW,

454 microbially-mediated weathering may be more resilient to cation scavenging by soil pools that
455 either delay or inhibit CDR (Figure 7).

456

457 **4.5. Cation mass-balance indicates increased silicate weathering in MP1-treated soils**

458 Combining results of the sequential extraction with cation fluxes measured in leachate, and base
459 cations in plant tissue, we found elevated masses of Ca, Mg, and K in the MP1-treated soils,
460 compared to UTC soils (Figure 6). Whereas the total mass of Na decreased in the MP1-treated
461 soils. Taken together, these results provide further support for MP1-driven acceleration of silicate
462 mineral weathering as the ultimate source of the additional cations. On average, the masses of
463 available Ca, Mg, and K in the MP1-treated soils were 6.3%, 2.7%, and 1.1% higher than in the
464 UTC columns, respectively. In contrast, there was a 9.6% reduction of available Na in the MP1-
465 treated columns. However, it should be noted that the magnitudes (Table S3) of MP1-driven
466 changes in Na (-10 mg col⁻¹) and K (+12 mg col⁻¹) were much smaller than Ca (+806 mg col⁻¹) or
467 Mg (+154 mg col⁻¹) and are therefore more likely to be explained by natural heterogeneity or by a
468 limited ability to detect small changes at low concentrations. In total, increases in base cations
469 equate to an average increase of 52.8 mEq of charge per column in the MP1-treated soils, with
470 plant, oxidizable, and leachate fractions accounting for a very small fraction of the total (Figure
471 6). This corresponds to a maximum CDR of 1.1 g CO₂ kg⁻¹ soil, assuming all cations from
472 increased silicate weathering are exported from the near field as alkalinity. Based on sequential
473 extraction data, the carbonate fraction accounted for 37% (19.5 mEq col⁻¹) of the overall increase,
474 which is very close to estimates for wollastonite weathering (soil pH = 5.16) reported in te Pas et
475 al. (2025). However, when SIC measurements are used to correct for the potential overextraction
476 of cations in the exchangeable step we estimate the carbonate fraction accounts for as much as

477 35.2 mEq col⁻¹ or 67% of new cations from silicate weathering. Carbonate is a less efficient sink
478 for weathering products than export of alkalinity (Figure 7), still the CDR associated with the
479 carbonate fraction accounts for between 0.20 and 0.36 g CO₂ kg⁻¹ soil and, importantly, it
480 corresponds to realized CDR.

481

482 **4.6. Considerations of the durability of CDR generated from MCM.**

483 Under field conditions, the fate of the accumulated carbonate will determine durability of the CDR
484 generated through the MCM approach. If the accumulated carbonates are stable, then the durability
485 of CDR will be at the least equivalent to their soil residence time, which can reach millennia (Landi
486 et al., 2003; Monger et al., 2015). On the other hand, if the accumulated carbonates redissolve,
487 then long-term CDR durability will hinge on whether the associated base cations are exported from
488 the system and transported to the ocean (as with traditional EW systems). Raymond, Planavsky,
489 and Reinhard (2025) note that carbonate dissolution in buffered soil systems results in the
490 production of bicarbonate (HCO₃⁻) rather than CO₂ outgassing. This is supported by field
491 observations from calcareous agricultural soils demonstrating that, even under active fertilization
492 and nitrification, abiotic CO₂ emissions were negligible (Hodges et al., 2021). Because we have
493 shown that the observed increases in soil carbonate derives from the microbially-mediated
494 acceleration of silicate weathering in a well-buffered soil, subsequent dissolution of the newly
495 formed carbonates would correspond to an additional mole of CDR for every mole of CaCO₃
496 dissolved, and the resulting dissolved inorganic carbon will be in the form of HCO₃⁻ not CO₂. This
497 implies that an MRV approach for MCM based on the accumulation of SIC represents a
498 conservative estimate of the carbon removal, and the resulting CDR is likely to be highly durable.
499

500 **5. CONCLUSIONS**

501 Our results further support the application of microbially-accelerated weathering, e.g., MCM, as a
502 viable method of CDR. The sequential selective dissolution measurements and cation mass balance
503 calculations provide strong evidence of silicate weathering increases associated with the MP1
504 treatment and confirm that secondary carbonate formation plays an important role in this process.
505 Because there was limited evidence of increased base cation or alkalinity export from the
506 experimental mesocosms, the exchangeable and carbonate pools were the primary sinks for
507 weathering derived based cations, with smaller but significant increases also observed in the
508 reducible pool.

509

510 By combining the soil sequential selective extraction with measurements of soil leachate and plant
511 biomass, we quantified the overall increase in base cations due to silicate weathering and traced
512 the fate of these weathering products (Figure 7). We show that between 37 and 67% of weathering
513 driven increases in base cations went to carbonate formation, with the remaining cations retained
514 mainly in the soil exchangeable pool that is assumed to delay CDR. At much smaller magnitudes,
515 the remaining cations were retained in the soil organic pool, representing potential future CDR and
516 in the soil reducible pool and plant fraction, which would constitute no CDR. The range reported
517 for carbonate reflects the possible overextraction of the exchangeable pool, which we constrained
518 with independent measurements of SIC. Our findings suggest caution should be used when
519 comparing sequential extraction results across soils spanning a wide range of pH. In soils with pH
520 greater than ~7, it is also advisable to measure SIC as an independent check on the magnitude of
521 the carbonate fraction.

522

523 These results also suggest an advantage of using SIC as the basis for measurement, reporting, and
524 verification (MRV) of CDR in these systems. Although there was a strong correlation between
525 base cation and SIC-based estimates of carbonates, SIC is easier and more cost effective to
526 measure, and in soils with higher pH it may also be more accurate. Furthermore, when MCM is
527 applied in well-buffered soils, an SIC-based MRV approach represents a conservative estimate of
528 CDR. While field-scale studies and modeling should be used to confirm the long-term durability
529 of CDR associated with MCM, the results presented here suggest this approach may have
530 significant benefits compared with traditional EW when applied under appropriate conditions.

531

532 **DATA AVAILABILITY**

533 The data described in this work are publicly archived and available (Fuenzalida-Meriz, 2026;
534 <https://doi.org/10.5281/zenodo.18420180>).

535

536 **ACKNOWLEDGMENTS**

537 The authors thank Dr. Sara Vicca (University of Antwerp) who contributed to early discussions of
538 the selective sequential extraction procedure and provided the laboratory facilities for that work.

539 **REFERENCES**

540

541 American Public Health Association. 1998. *Standard Methods for the Examination of Water and*
542 *Wastewater*. Vol. 6. 20th Edition, American Public Health Association (APHA).

543

544 Banfield, J. F., Barker, W. W., Welch, S. A., & Taunton, A. 1999. Biological impact on mineral
545 dissolution: application of the lichen model to understanding mineral weathering in the
546 rhizosphere. *Proceedings of the National Academy of Sciences*, 96(7), 3404-3411.

547

548 Berner, R. A. 1997. Paleoclimate - The rise of plants and their effect on weathering and
549 atmospheric CO₂. *Science*, 276(5312), 544–546.

550

551 Bijma, J., Hagens, M., Hammes, J.S., Planavsky, N., Strandmann, P.A.E.P. von, Reershemius, T.,
552 Reinhard, C.T., Renforth, P., Suhrhoff, T.J., Vicca, S., Vienne, A., Wolf-Gladrow, D., 2025.
553 Reviews and syntheses: Carbon vs. cation based MRV of Enhanced Rock Weathering and the
554 issue of soil organic carbon. *Biogeosciences* 23, 53–75. <https://doi.org/10.5194/bg-23-53-2026>

555

556 Clarkson, M. O., Larkin, C. S., Swoboda, P., Reershemius, T., Suhrhoff, T. J., Maesano, C. N., &
557 Campbell, J. S. 2024. A review of measurement for quantification of carbon dioxide removal by
558 enhanced weathering in soil. *Frontiers in Climate*, 6, 1345224.

559

560 Climate Change 2022: Mitigation of Climate Change. Contribution of Working Group III to the
561 Sixth Assessment Report of the Intergovernmental Panel on Climate Change. Cambridge
562 University Press.

563

564 Combs, S. M., and M. V. Nathan. 1998. "Soil Organic Matter." In *Recommended Chemical Soil*
565 *Test Procedures for the North Central Region*, edited by J. R. Brown, vol. 221, 53–58. Missouri
566 Agriculture Experiment Station.

567

568 Corbett, T., Odelius, E., Uebel, T., Jonsson, T., Singh, A., Vicca, S., Hagens, M., Budnyak, T.,
569 Tkachenko, O., Poetra, R., Hartmann, J., Janssens, I., Niron, H., Van Tendeloo, M., Vlaeminck,
570 S., & Neubeck, A. 2025. Microbial dissolution of Gran Canaria lapilli in small-scale flow through
571 columns: carbon dioxide removal potential. *npj Materials Degradation*, 9(1), 60.

572

573 Domínguez-Villar, D., Bensa, A., Švob, M., & Krklec, K. 2022. Causes and implications of the
574 seasonal dissolution and precipitation of pedogenic carbonates in soils of karst regions—A
575 thermodynamic model approach. *Geoderma*, 423, 115962.

576

577 Dong, H., Huang, L., Zhao, L., Zeng, Q., Liu, X., Sheng, Y., Shi, L., Wu, G., Jiang, H., Li, F.,
578 Zhang, L., Guo, D., Li, G., Hou, W., & Chen, H. 2022. A critical review of mineral–microbe
579 interaction and co-evolution: mechanisms and applications. *National Science Review*, 9(10),
580 nwac128. <https://doi.org/10.1093/nsr/nwac128>

581

582 Fierer, N., & Walsh, C. M. 2023. Can we manipulate the soil microbiome to promote carbon
583 sequestration in croplands? *PLoS Biology*, 21(7), e3002207.

584

585 Finlay, R.D., Mahmood, S., Rosenstock, N., Bolou-Bi, E.B., Köhler, S.J., Fahad, Z., Rosling, A.,
586 Wallander, H., Belyazid, S., Bishop, K., Lian, B., 2020. Reviews and syntheses: Biological
587 weathering and its consequences at different spatial levels—from nanoscale to global scale.
588 *Biogeosciences* 17, 1507–1533. <https://doi.org/10.5194/bg-17-1507-2020>

589

590 Fuenzalida-Meriz, G. A. 2026. Dataset for manuscript "Tracing the cation budget of microbially-
591 accelerated weathering from silicates to soil carbonates" [Data set].
592 Zenodo. <https://doi.org/10.5281/zenodo.18420180>

593

594 Hasemer, H., Borevitz, J., & Buss, W. 2024. Measuring enhanced weathering: inorganic carbon-
595 based approaches may be required to complement cation-based approaches. *Frontiers in Climate*,
596 6, 1352825.

597

598 Hass, A., & Fine, P. 2010. Sequential selective extraction procedures for the study of heavy metals
599 in soils, sediments, and waste materials—a critical review. *Critical Reviews in Environmental*
600 *Science and Technology*, 40(5), 365-399.

601

602 Heckman, K., Lawrence, C. R., & Harden, J. W. 2018. A sequential selective dissolution method
603 to quantify storage and stability of organic carbon associated with Al and Fe hydroxide phases.
604 *Geoderma*, 312, 24-35.

605

606 Hodges, C., Brantley, S. L., Sharifironizi, M., Forsythe, B., Tang, Q., Carpenter, N., & Kaye, J.
607 2021. Soil carbon dioxide flux partitioning in a calcareous watershed with agricultural impacts.
608 *Journal of Geophysical Research: Biogeosciences*, 126(10), e2021JG006379.

609

610 Johnson, D., Hooper, P., & Conrey, R. 1999) XRF method XRF analysis of rocks and minerals for
611 major and trace elements on a single low dilution Li-tetraborate fused bead. *Advances in X-ray*
612 *Analysis*, 41, 843-867.

613

614 Johnstone, I., Fuss, S., Walsh, N., & Höglund, R. 2025. Carbon markets for carbon dioxide
615 removal. *Climate Policy*, 1–8.

616

617 Kelly, D.S. 2018. Analysis of Geological Materials by Low Dilution Fusion at the Peter Hooper
618 GeoAnalytical Lab (Washington State University). Washington State University, Pullman, WA,
619 USA.

620

621 Landi, A., Mermut, A. R., & Anderson, D. W. 2003. Origin and rate of pedogenic carbonate
622 accumulation in Saskatchewan soils, Canada. *Geoderma*, 117(1–2), 143–156.

623

624 Maher, K., Steefel, C. I., White, A. F., & Stonestrom, D. A. 2009. The role of reaction affinity and
625 secondary minerals in regulating chemical weathering rates at the Santa Cruz Soil
626 Chronosequence, California. *Geochimica et Cosmochimica Acta*, 73(10), 2804-2831.

627

628 Manning, D. A., & Renforth, P. 2013. Passive sequestration of atmospheric CO₂ through coupled
629 plant-mineral reactions in urban soils. *Environmental Science & Technology*, 47(1), 135-141.
630

631 Martin, J. M., Nirel, P., & Thomas, A. J. 1987. Sequential extraction techniques: promises and
632 problems. *Marine Chemistry*, 22(2-4), 313-341.
633

634 McConnaughey, T. A., & Whelan, J. F. 1997. Calcification generates protons for nutrient and
635 bicarbonate uptake. *Earth-Science Reviews*, 42(1-2), 95-117.
636

637 Monger, H. C., Kraimer, R. A., Khresat, S. E., Cole, D. R., Wang, X., & Wang, J. 2015.
638 Sequestration of inorganic carbon in soil and groundwater. *Geology*, 43(5), 375-378.
639

640 Nel, T., Bruneel, Y., & Smolders, E. 2023. Comparison of five methods to determine the cation
641 exchange capacity of soil. *Journal of Plant Nutrition and Soil Science*, 186(3), 311-320.
642

643 Nelson, D. W., and L. E. Sommers. 1996. "Total Carbon, Organic Carbon, and Organic Matter."
644 In *Methods of Soil Analysis: Part 3 Chemical Methods*, edited by D. L. Sparks, A. L.
645

646 Niron, H., Vienne, A., Frings, P., Poetra, R., & Vicca, S. 2024. Exploring the synergy of enhanced
647 weathering and *Bacillus subtilis*: A promising strategy for sustainable agriculture. *Global Change*
648 *Biology*, 30(9), e17511.
649

650 Niron, H., Calogiuri, T., Singh, A., Neubeck, A., Tendeloo, M.V., Cox, T., Hartmann, J.,
651 Vlaeminck, S.E., Vicca, S., 2025. Alkalinity production and carbon capture from dunite
652 weathering: Individual effects of oxalate, citrate, and EDTA salts. *Chem. Eng. J. Adv.* 24, 100902.
653 <https://doi.org/10.1016/j.ceja.2025.100902>
654

655 Peters, J. B., M. V. Nathan, C. A. M. Laboski, and M. Nathan. 2012. “pH and Lime Requirement.
656 Ch. 4.” *In Recommended Chemical Soil Test Procedures for the North Central Region*, vol. 221,
657 16–22. University of Missouri.

658

659 R Core Team 2021. R: A language and environment for statistical computing. *R Foundation for*
660 *Statistical Computing*, Vienna, Austria. URL <https://www.R-project.org/>.

661

662 Raymond, P., Planavsky, N., & Reinhard, C. T. 2025. Using carbonates for carbon removal. *Nature*
663 *Water*, 3(8), 844-847.

664

665 Ribeiro, I. D. A., Volpiano, C. G., Vargas, L. K., Granada, C. E., Lisboa, B. B., & Passaglia, L.
666 M. P. 2020. Use of mineral weathering bacteria to enhance nutrient availability in crops: a review.
667 *Frontiers in Plant Science*, 11, 590774.

668

669 Richards, L. A., ed. 1954. *Diagnosis and Improvement of Saline and Alkali Soils (No. 60)*. US
670 Government Printing Office.

671

672 Smith, S. M., Geden, O., Gidden, M. J., Lamb, W. F., Nemet, G. F., Minx, J. C., Buck, H., Burke,
673 J., Cox, E., Edwards, M. R., Fuss, S., Johnstone, I., Müller-Hansen, F., Pongratz, J., Probst, B. S.,
674 Roe, S., Schenuit, F., Schulte, I., Vaughan, N. E. (eds.) *The State of Carbon Dioxide Removal 2024*
675 - 2nd Edition. DOI 10.17605/OSF.IO/F85QJ, 2024.

676

677 Samuels et al. 2020, Microbial weathering of minerals and rocks in natural environments. In:
678 Dontsova K, Balogh-Brunstad Z, Roux GL (eds.). *Biogeochemical Cycles: Ecological Drivers*
679 *and Environmental Impact*. Hoboken and Washington, DC: Wiley, 59–79.

680

681 Steinwigger, L., Boito, L., Frings, P.J., Niron, H., Rijnders, J., Schutter, A. de, Vienne, A., Vicca,
682 S., 2025. Beyond Inorganic C: Soil Organic C as a Key Pathway for Carbon Sequestration in
683 Enhanced Weathering. *Global Change Biology* 31, e70340.

684

685 Steinwigger, L., Boito, L., de Schutter, A., Frings, P. J., Miladinović, N., Niron, H., ... & Vicca, S.
686 2026. Higher Inorganic CO₂ Removal Despite Slower Weathering in an Enhanced Weathering
687 Experiment With Steel Slags and Basalt. *Global Change Biology*, 32(1), e70666.

688

689 Sumner, M. E., and W. P. Miller. 1996. "Cation Exchange Capacity and Exchange Coefficients."
690 In *Methods of Soil Analysis: Part 3 Chemical Methods*, edited by D. L. Sparks, A. L. Page, P. A.
691 Helmke, et al., vol. 5, 1201–1229. American Society of Agronomy, Crop Science Society of
692 America, and Soil Science Society of America.

693

694 Supuran, C. T. 2016. Structure and function of carbonic anhydrases. *Biochemical Journal*,
695 473(14), 2023-2032.

696

697 te Pas, E. E. E. M. te, Chang, E., Marklein, A. R., Comans, R. N. J., & Hagens, M. 2025.
698 Accounting for retarded weathering products in comparing methods for quantifying carbon dioxide
699 removal in a short-term enhanced weathering study. *Frontiers in Climate*, 6, 1524998.

700

701 Timmermann, T., Yip, C., Yang, Y., Wemmer, K.A., Chowdhury, A., Dores, D., Takayama, T.,
702 Nademanee, S., Traag, B.A., Zamanian, K., González, B., Breecker, D.O., Fierer, N., Slessarev,
703 E.W., Fuenzalida-Meriz, G.A. 2025. Harnessing Microbes to Weather Native Silicates in
704 Agricultural Soils for Scalable Carbon Dioxide Removal. *Global Change Biology* 31(5), e70216.

705

706 Tessier, A. P. G. C., Campbell, P. G., & Bisson, M. J. A. C. 1979. Sequential extraction procedure
707 for the speciation of particulate trace metals. *Analytical Chemistry*, 51(7), 844-851.

708

709 Tosca, N.J. & Tutolo, B.M., 2023. Alkalinity in Theory and Practice. *Elements* 19, 7–9.

710

711 Uhlig, D., & Von Blanckenburg, F. 2019. How slow rock weathering balances nutrient loss during
712 fast forest floor turnover in montane, temperate forest ecosystems. *Frontiers in Earth Science*, 7,
713 159.

714

715 Uroz, S., Calvaruso, C., Turpault, M. P., & Frey-Klett, P. 2009. Mineral weathering by bacteria:
716 ecology, actors and mechanisms. *Trends in Microbiology*, 17(8), 378-387.

717

718 Verbruggen, E., Struyf, E., & Vicca, S. 2021. Can arbuscular mycorrhizal fungi speed up carbon
719 sequestration by enhanced weathering? *Plants, People, Planet*, 3(5), 445-453.

720

721 Vicca, S., Goll, D. S., Hagens, M., Hartmann, J., Janssens, I. A., Neubeck, A., ... & Verbruggen,
722 E. 2022. Is the climate change mitigation effect of enhanced silicate weathering governed by
723 biological processes?. *Global Change Biology*, 28(3), 711-726.

724

725 Vienne, A., Frings, P., Rijnders, J., Suhrhoff, T.J., Reershemius, T., Poetra, R.P., Hartmann, J.,
726 Niron, H., Estrada, M.P., Steinwidder, L., Boito, L., Vicca, S., 2025. Weathering without inorganic
727 CDR revealed through cation tracing. *EGUsphere* 2025, 1–24. doi:10.5194/egusphere-2025-1667

728

729 Wagai, R., & Mayer, L. M. 2007. Sorptive stabilization of organic matter in soils by hydrous iron
730 oxides. *Geochimica et Cosmochimica Acta*, 71(1), 25-35.

731

732 Walker, J. C. G., Hays, P. B., & Kasting, J. F. 1981. A negative feedback mechanism for the long-
733 term stabilization of Earth's surface temperature. *Journal of Geophysical Research*, 86(C10):
734 9776–9782.

735

736 Wild, B., Gerrits, R., & Bonneville, S. 2022. The contribution of living organisms to rock
737 weathering in the critical zone. *npj Materials degradation*, 6(1), 98.

738

739 Wickham H, Averick M, Bryan J, Chang W, McGowan LD, François R, Grolemund G, Hayes A,
740 Henry L, Hester J, Kuhn M, Pedersen TL, Miller E, Bache SM, Müller K, Ooms J, Robinson D,
741 Seidel DP, Spinu V, Takahashi K, Vaughan D, Wilke C, Woo K, Yutani H. 2019. Welcome to
742 the tidyverse. *Journal of Open Source Software*, 4(43), 1686. doi:10.21105/joss.01686.
743

744 Wright, V. P. 1989. Terrestrial stromatolites and laminar calcretes: a review. *Sedimentary*
745 *Geology*, 65(1-2), 1-13.
746

747 Xiao, L., Lian, B., Hao, J., Liu, C., & Wang, S. 2015. Effect of carbonic anhydrase on silicate
748 weathering and carbonate formation at present day CO₂ concentrations compared to primordial
749 values. *Scientific Reports*, 5(1), 7733.
750

751 Yang, Y. Y., de Mesquita, C. P. B., Lawrence, C. R., Weyman, P. D., Dores, D., Timmermann,
752 T., Fierer, N., & Fuenzalida-Meriz, G. A. 2026. Synergistic Effects of a Microbial Amendment
753 and Crushed Basalt: Soil Geochemical and Microbial Responses. *Global Change Biology* 32(1),
754 e70705.
755

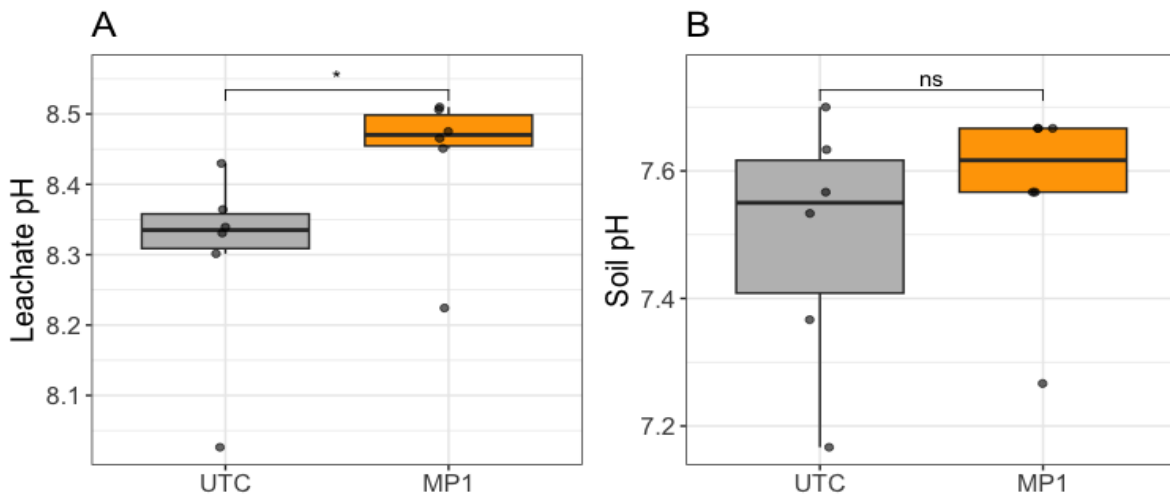
756 Yip, C., Weyman, P. D., Wemmer, K. A., Yang, Y. Y., Chowdhury, A., Traag, B. A.,
757 Timmermann, T., & Fuenzalida-Meriz, G. 2025. Quantification of soil inorganic carbon using
758 sulfamic acid and gas chromatography. *PLoS One*, 20(5), e0320778.
759

760 Zhu T and Dittrich M. 2016. Carbonate Precipitation through Microbial Activities in Natural
761 Environment, and Their Potential in Biotechnology: A Review. *Frontiers in Bioengineering and*
762 *Biotechnology*. 4:4. doi: 10.3389/fbioe.2016.00

763

764 **FIGURES**

765

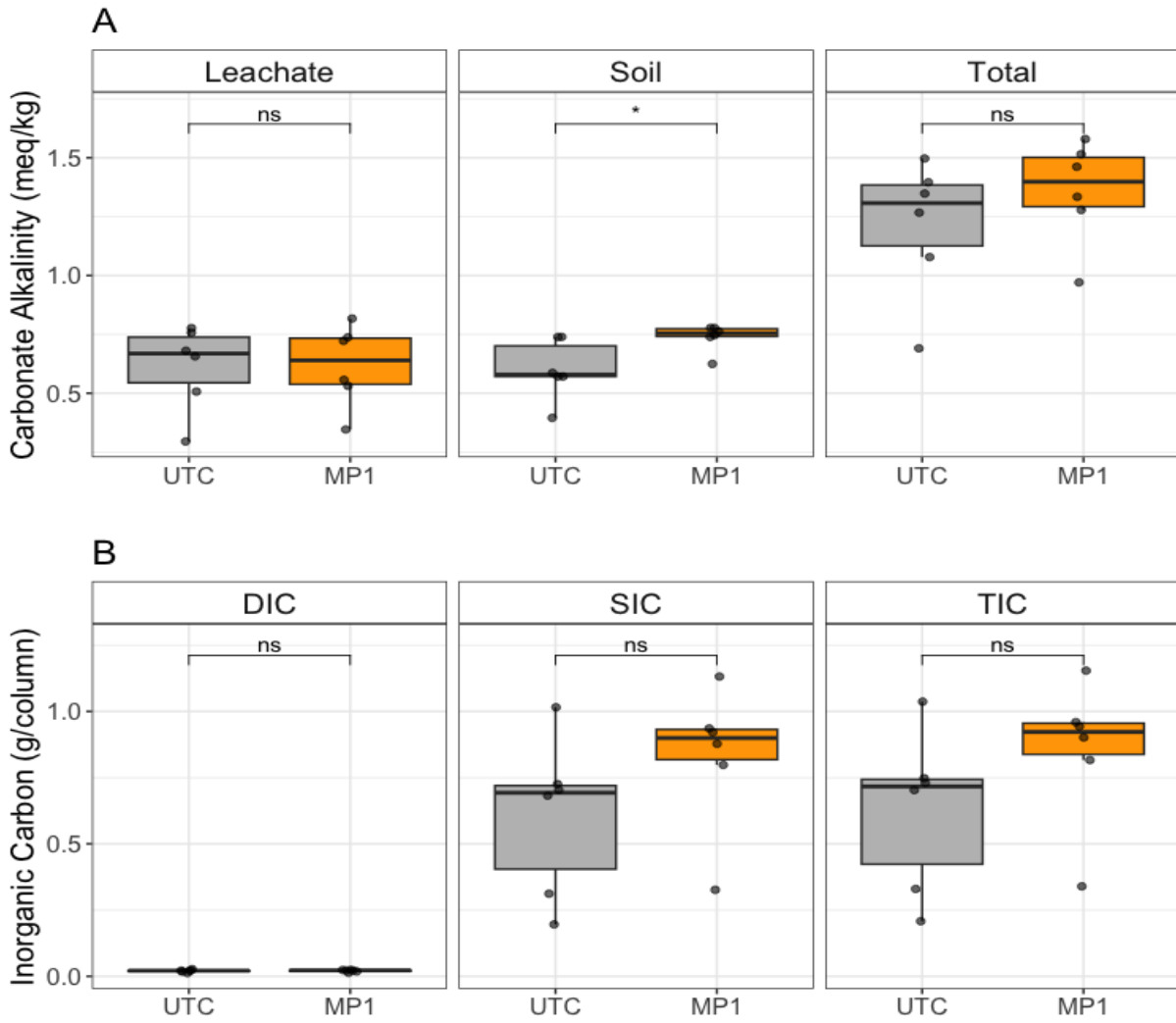


766

767 **Figure 1.** Leachate pH (A) and soil pH (B) in MP1-treated and untreated control (UTC) columns.

768 Wilcoxon signed-rank test, * $p < 0.05$, ns: not significant, $N = 6$. Note that y-axes are scaled to the

769 data range to clearly visualize the distribution and variability across treatments.

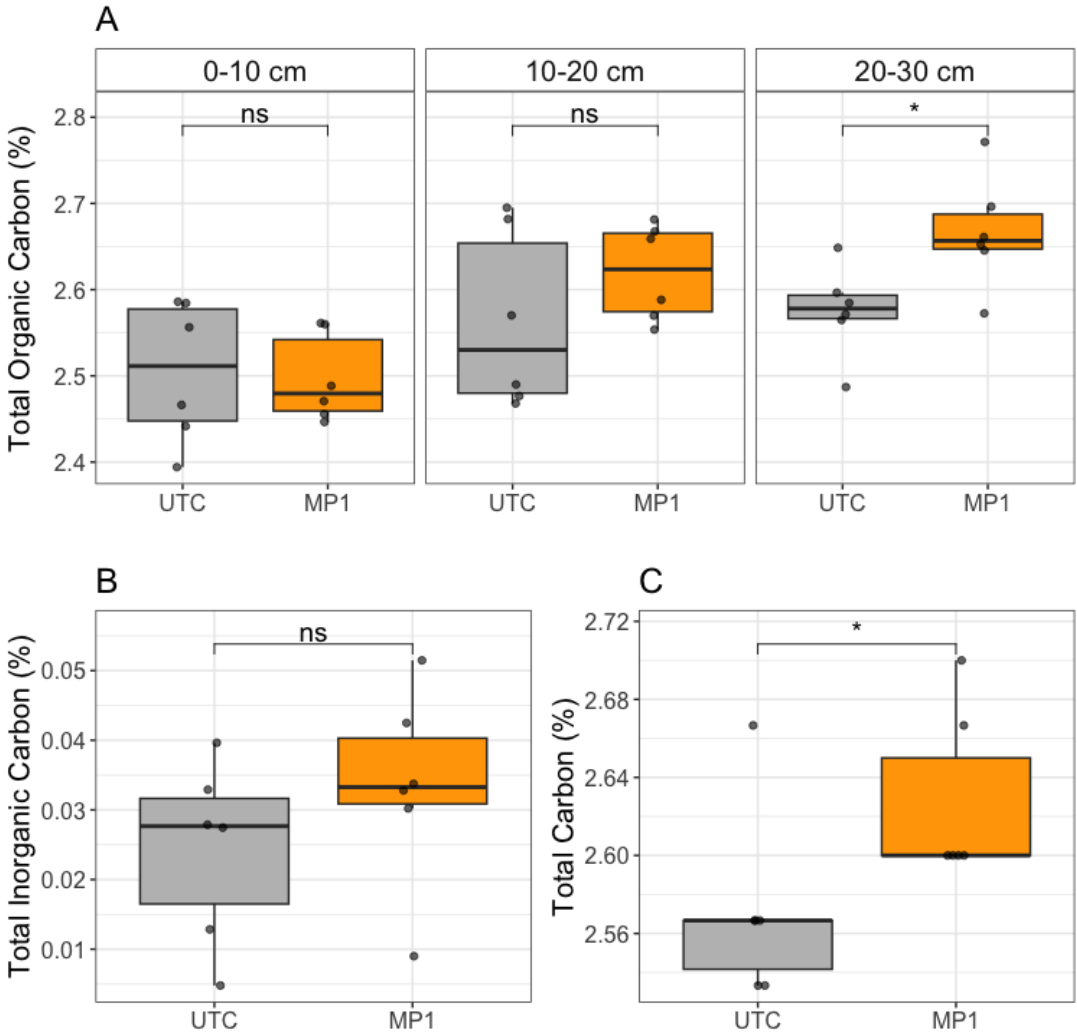


770

771 **Figure 2.** Carbonate alkalinity (**A**) and inorganic carbon (**B**) in MP1-treated and untreated control

772 (UTC) columns. Student's t-test, * $p < 0.05$, ns: not significant, $N = 6$.

773



774

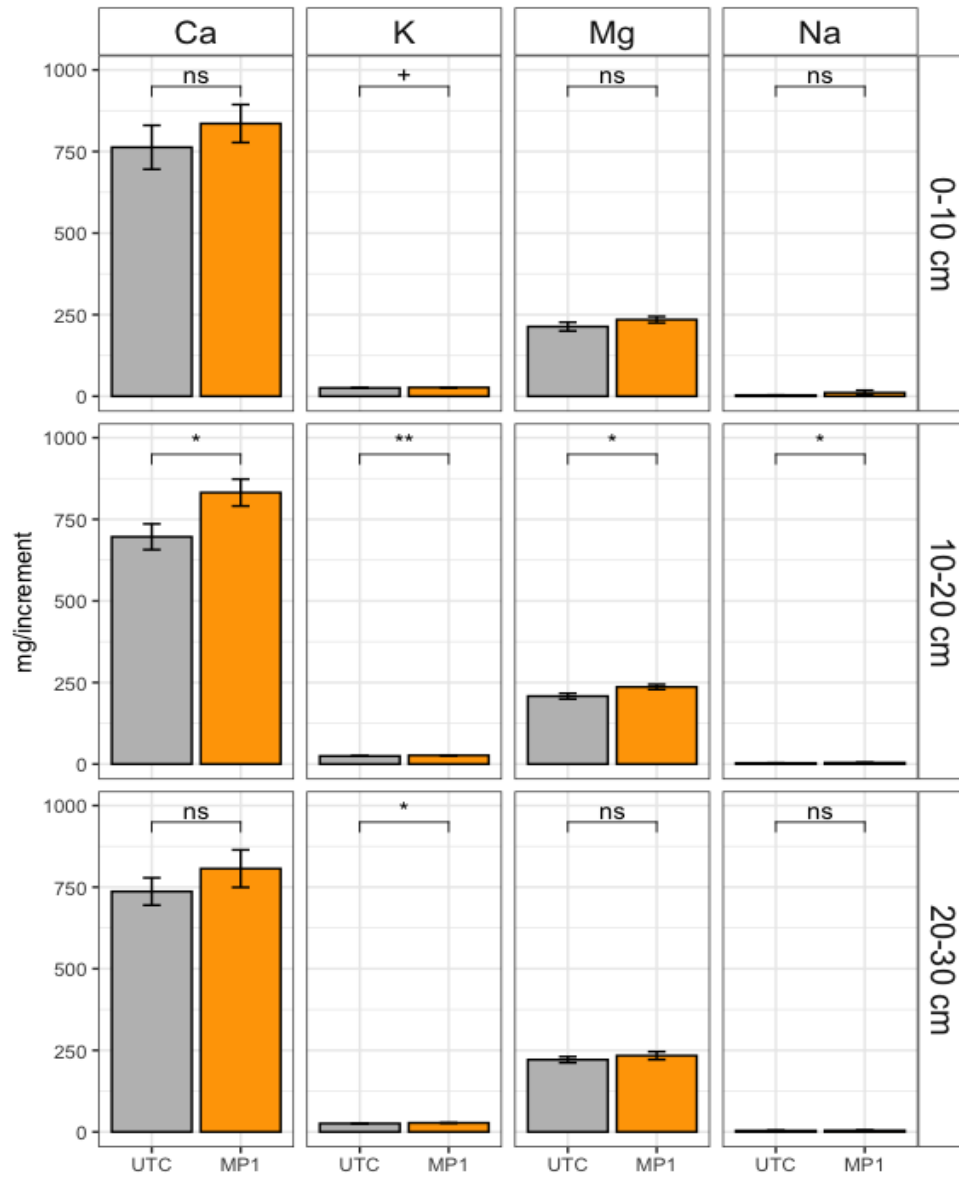
775 **Figure 3.** Total organic carbon (A), total inorganic carbon (B) and total carbon (C) in MP1-treated

776 and untreated control (UTC) columns. Wilcoxon signed-rank test, * $p < 0.05$, ns: not significant,

777 $N = 6$. Note that y-axes are scaled to the data range to clearly visualize the distribution and

778 variability across treatments.

779

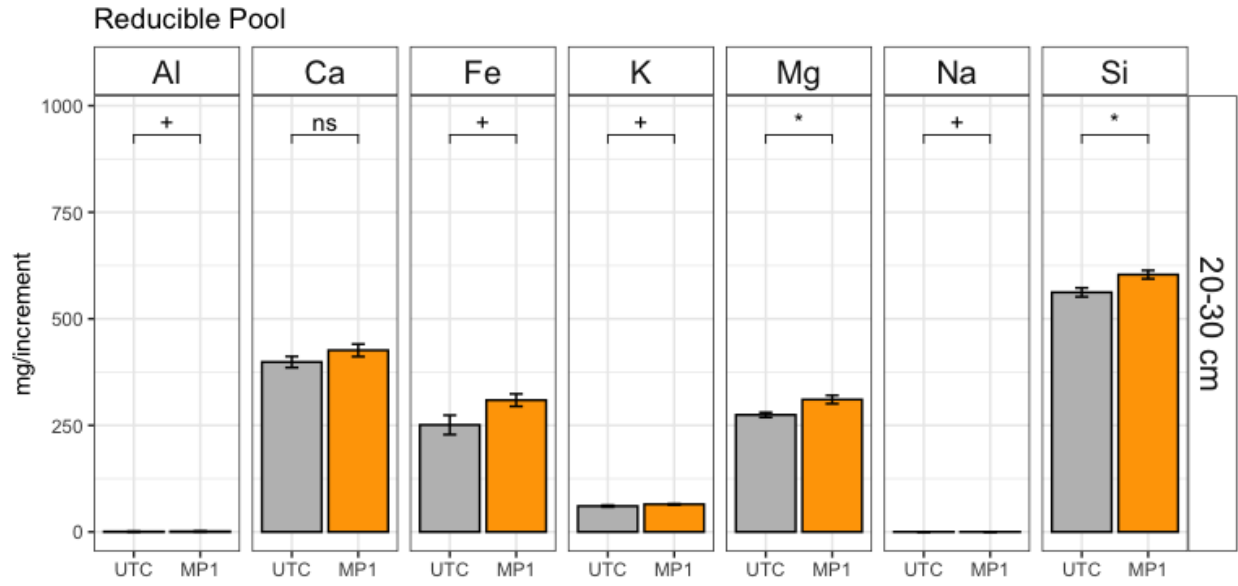


780

781 **Figure 4.** Concentration per depth increment of base cations in the carbonate pool in MP1-treated

782 and untreated control (UTC) columns. Student's t-test, * $p < 0.05$, ns: not significant, $N = 6$.

783

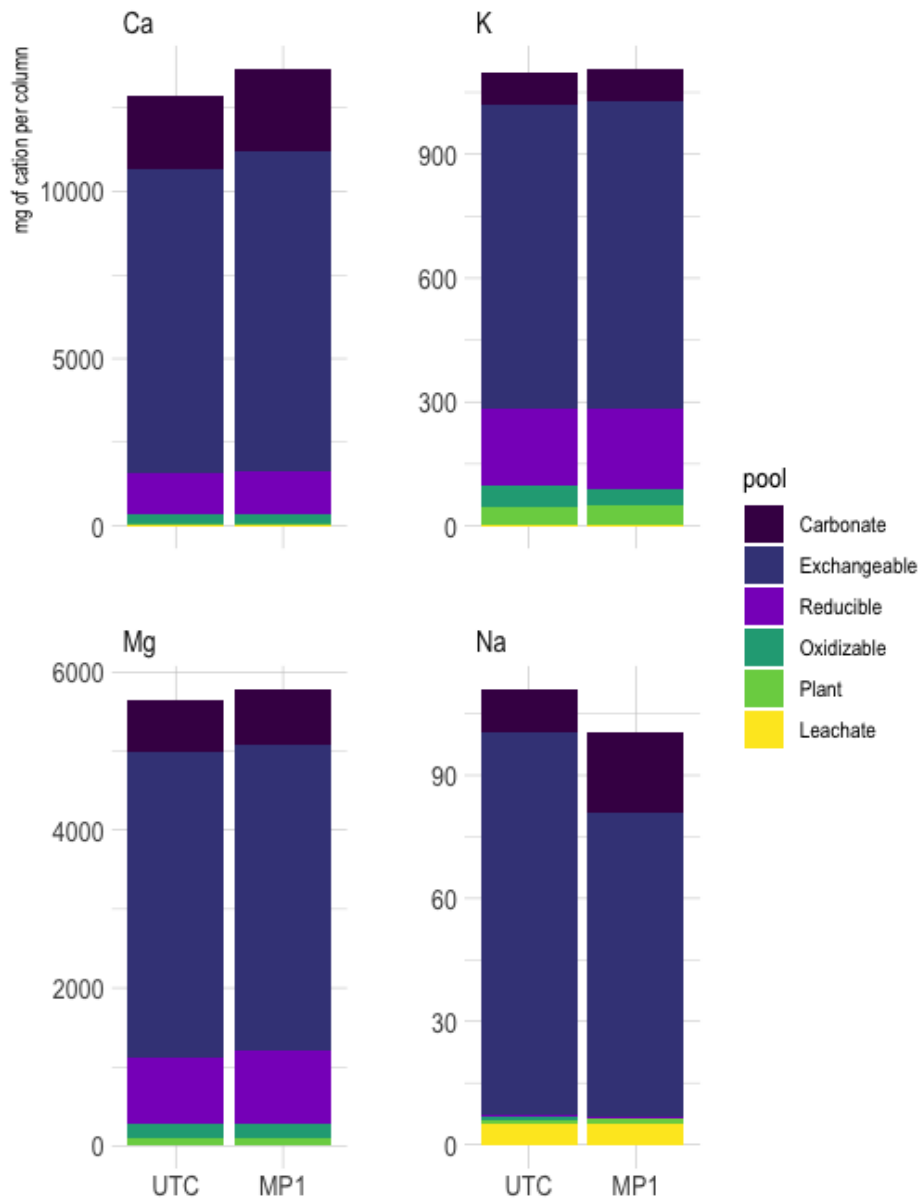


784

785 **Figure 5.** Concentration at the bottom depth of base cations in the reducible pool in MP1-treated

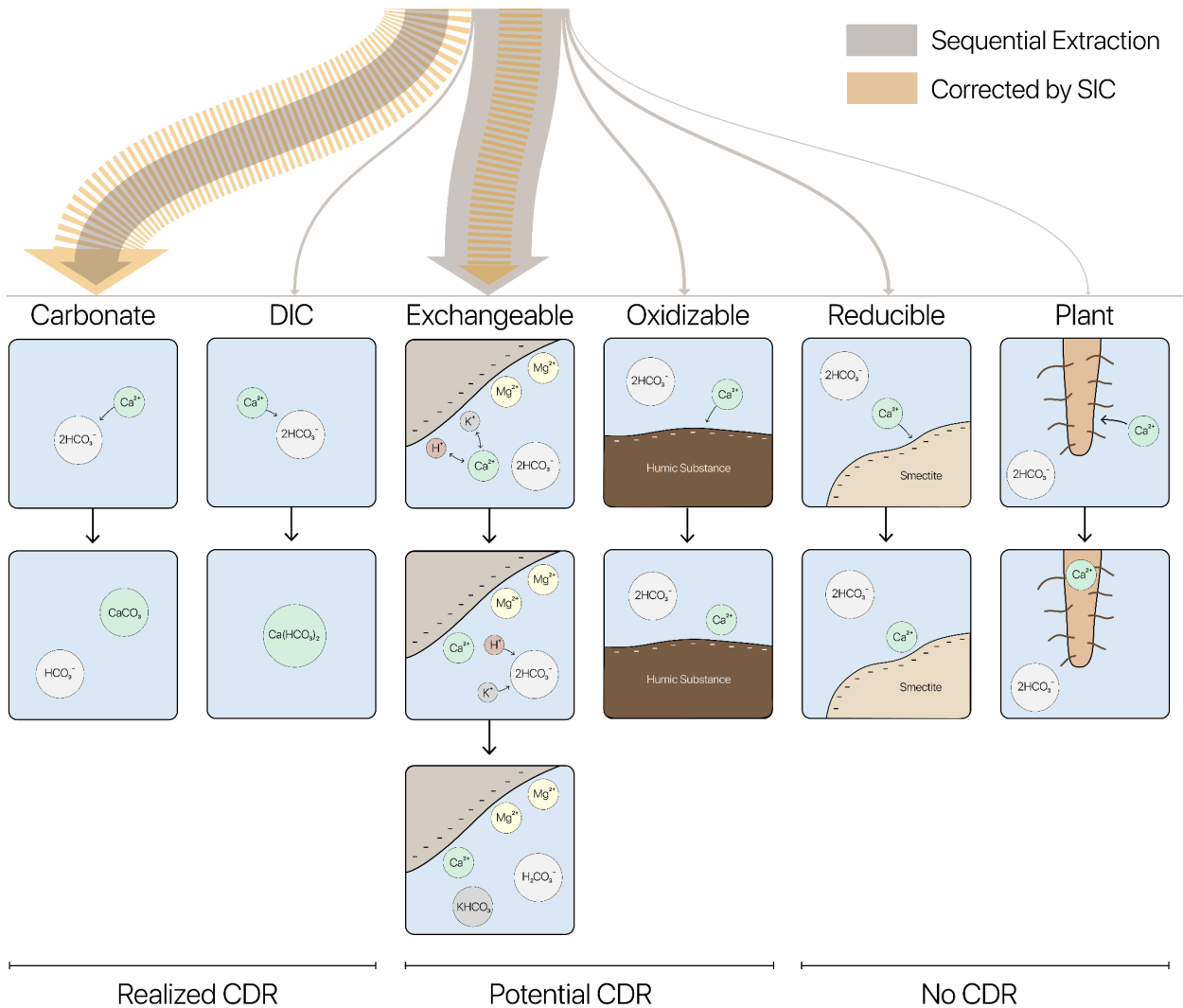
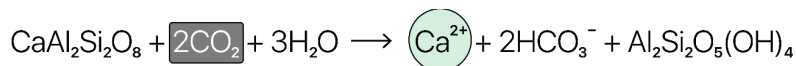
786 and untreated control (UTC) columns. Student's t-test, * $p < 0.05$, ns: not significant, $N = 6$.

787



788

789 **Figure 6.** Cation mass-balance. Total mass of cations (in mg) per column, and their distribution
 790 between measured pools at the end of the 63-day experimental period. The carbonate,
 791 exchangeable, reducible, and oxidizable fractions are based on selective sequential extraction
 792 measurements.



793

794

795

796

797

798

799

800

801

Figure 7. The mass balance approach reported here allows for tracking the fate of the observed increases in base cations from the acceleration of silicate weathering by the *B. subtilis* strain MP1. For simplification, we assume the observed increase in Ca ions is derived from the dissolution of anorthite mineral, and that the resulting Ca ions end up in one of six possible soil fractions: Carbonate, DIC, Exchangeable, Oxidizable, Reducible and Plant. The width of the gray arrows is proportional to the amount of new Ca ions that end up in one of the six characterized soil fractions. The width of the yellow arrows is proportional to the amount of new Ca ions that end up in the exchangeable and carbonate pools, corrected by the soil inorganic carbon measurement. Only Ca

802 ions that end up in the carbonate pool or are exported as dissolved inorganic carbon constitute
803 realized CDR. The exchangeable and oxidizable pools constitute potential future CDR, while the
804 reducible and plant pools represent cation scavenging that do not lead to CDR (no CDR).